Available online at www.sciencedirect.com

ScienceDirect

Advances in Space Research 70 (2022) 2383–2398

ADVANCES IN SPACE RESEARCH (a COSPAR publication)

www.elsevier.com/locate/asr

Earth rotation parameter estimation from LLR

Vishwa Vijay Singh [a,b,*], Liliane Biskupek [a], Jürgen Müller [a], Mingyue Zhang [a,b]

[a] Institute of Geodesy (IfE), Leibniz University Hannover, Schneiderberg 50, 30167 Hannover, Germany
[b] Institute for Satellite Geodesy and Inertial Sensing, German Aerospace Center (DLR), Callinstraße 36, 30167 Hannover, Germany

Received 27 October 2021; received in revised form 10 June 2022; accepted 15 July 2022
Available online 22 July 2022

Abstract

Lunar Laser Ranging (LLR) measures the distance between observatories on Earth and retro-reflectors on Moon since 1969. In this paper, we estimate the Earth Rotation Parameters (ERP; terrestrial pole offsets, x_p and y_p, and Earth rotation phase, ΔUT1) using LLR data. We estimate the values of ΔUT1, and the pole offsets separately for nights selected from subsets of the LLR time series which have a minimum of 5, 10, and 15 normal points obtained per night. For the pole offsets, we estimate the values of x_p and y_p simultaneously as well as separately. Overall, the uncertainties of ERP from the new LLR data (after 2000.0) have significantly improved compared to ERP from LLR data reported previously by Biskupek (2015) and Hofmann et al. (2018). The Weighted Root Mean Square (WRMS) value (after 2000.0) of the uncertainty for estimation of ΔUT1 lies between 17.03 μs and 24.49 μs for different subsets of nights. The WRMS values (after 2000.0) of the uncertainty for estimation of the terrestrial pole coordinates (estimated separately) for different subsets of nights lie between 1.30 mas and 3.46 mas for x_p and between 1.63 mas and 4.21 mas for y_p. The WRMS of differences between the estimated ΔUT1 values from LLR analysis and those from the a-priori ERP series lie between 59.38 μs and 115.35 μs for a subset of NPs from all LLR observatories post 2000.0. For x_p, the differences are between 1.18 mas and 2.18 mas, and for y_p, the differences are between 1.01 mas and 1.76 mas (x_p and y_p estimated separately). The differences of the obtained ERP from LLR analysis to the a-priori ERP series (for all subsets) become smaller with a stricter selection criteria (i.e. more number of NPs per night). Additionally, we see that the simultaneous estimation of the terrestrial pole offsets leads to high correlations between the estimated values of x_p and y_p of the same night. Furthermore, we estimate that the addition of non-tidal loading improves the uncertainties (3σ values) of the estimated ERPs by about 1%.

Keywords: Lunar laser ranging; Earth rotation parameters; Non-tidal loading

1. Introduction

Lunar Laser Ranging (LLR) is the measurement of round trip travel times of short laser pulses between observatories on the Earth and retro-reflectors on the Moon, first made possible after the Apollo 11 landing in 1969. As of 2022, there are five retro-reflectors on the Moon, and measurements have primarily been carried out from six observatories on the Earth that were or are capable to range to the Moon: the Côte d'Azur Observatory, France (OCA), the McDonald Laser Ranging Station, USA (MLRS), the Apache Point Observatory Lunar Laser ranging Operation, USA (APOLLO), the Lure Observatory on Maui island, Hawaii, USA (LURE), the Matera Laser Ranging Observatory, Italy (MLRO), and the Geodetic Observatory Wettzell, Germany (WLRS). As the amount of signal loss of the laser pulse is enormous, a series of single measurements over 5–15 min is used to calculate a so called normal point (NP). Details of the LLR measurement

* Corresponding author at: Institute of Geodesy (IfE), Leibniz University Hannover, Schneiderberg 50, 30167 Hannover, Germany
E-mail addresses: singh@ife.uni-hannover.de (V.V. Singh), biskupek@ife.uni-hannover.de (L. Biskupek), mueller@ife.uni-hannover.de (J. Müller), zhang@ife.uni-hannover.de (M. Zhang).

https://doi.org/10.1016/j.asr.2022.07.038
0273-1177/

process can be found, for example, in Murphy (2013) and Müller et al., (2019). LLR being the longest observation time series of all space geodetic techniques (Müller et al., 2019) allows the determination of a variety of parameters of the Earth–Moon dynamics, such as the mass of the Earth–Moon system, the lunar orbit and libration parameters (Williams et al., 2013 and Pavlov et al., 2016), terrestrial and celestial reference frames and coordinates of observatories and reflectors (Müller et al., 2009; Hofmann et al., 2018) etc. Additionally, it leads to improvements in the solar system ephemerides (Kopeikin et al., 2008; Folkner et al., 2014; Pavlov et al., 2016), selenophysics (Murphy, 2013; Hofmann, 2017; Viswanathan et al., 2019), and gravitational physics (Williams et al., 2006; Müller et al., 2012; Hofmann and Müller, 2018; Zhang et al., 2020; Biskupek et al., 2021). Furthermore, LLR can also be used to provide tests of Earth Orientation Parameters (EOPs) (Biskupek, 2015; Hofmann et al., 2018). The EOP values are combined from different space geodetic techniques (Bizouard et al., 2018), such as Very Long Baseline Interferometry (VLBI), Global Navigation Satellite System (GNSS), Satellite Laser Ranging (SLR), and Doppler Orbitography and Radiopositioning Integrated by Satellite (DORIS), and published by the Earth Orientation Centre of the International Earth Rotation and Reference Systems Service (IERS) and can be found at (http://www.iers.org/IERS/EN/DataProducts/EarthOrientationData/eop.html) and (https://hpiers.obspm.fr/eop-pc/index.php?index=C04&lang=en). LLR products are not yet a part of the EOPs published by the IERS (as IERS EOP 14 C04 series). The Kalman Earth Orientation Filter (KEOF) COMB series, of Ratcliff & Gross (2020), exists as an alternative to the IERS C04 series. It includes data from LLR in addition to those from SLR, VLBI, and GNSS.

As all space geodetic techniques use different observation techniques, are differently sensitive to the EOPs, and have different networks, the obtained EOPs from the space geodetic techniques are also different. These differences are further discussed in Section 2.3, Section 3.1, and Section 4.1. The absolute values of the Earth rotation phase (ΔUT1) can only be obtained from VLBI with the highest accuracy. The estimation of ΔUT1 values from satellite geodetic techniques (such as SLR, GNSS, etc.) is affected by long-term systematic errors (Gambis et al., 2011), mainly caused by effects of the long-wavelength Earth gravity field on satellite orbits (i.e. mainly due to C20), therefore their estimated ΔUT1 values are commonly not used to verify the results of VLBI. For LLR, this systematic error effect is much less relevant, as the perturbation of the lunar orbit (compared to artificial satellites) due to C20 of the Earth is not very high. Therefore, space geodetic techniques other than LLR are not suited for any reasonable comparison of ΔUT1 with VLBI.

In this study, we estimate the ΔUT1 and the terrestrial pole offsets (x_p and y_p, hereon referred to as polar motion coordinates (PMC)) values using LLR data (together with the Length-of-Day, they are referred to as the Earth Rotation Parameters (ERPs)). Section 2 defines the data and methods of calculations used for the estimation of ΔUT1 (in Section 3), and x_p and y_p (in Section 4). In Section 3 and Section 4, we give the most recent results and discuss the uncertainty of the ERPs, analyse the correlations of the estimated parameters with each other, and additionally study the effect of non-tidal loading (NTL) on the estimated values of x_p and y_p, and ΔUT1. In Section 5, we give the conclusions to this study.

2. Data and method

In Germany, from the early 80ies, the software package LUNAR (LUNar laser ranging Analysis softwaRe) has been developed to study the Earth-Moon system and to determine several related model parameters (Egger, 1985; Gleixner, 1986; Bauer, 1989; Müller, 1991). The analysis model used in LUNAR is based on Einstein's theory of relativity. It is fully relativistic and complete up to the first post-Newtonian ($1/c^2$) level. To take advantage of the high-precision NPs that can be obtained with an accuracy of several millimetres (Murphy, 2013), the LUNAR software was updated continuously (Biskupek, 2015; Hofmann, 2017). A recent overview of LUNAR is given in Hofmann et al. (2018), a detailed description can be found in Müller et al. (2014). With a least-squares adjustment, in the current version of LUNAR, up to 200 unknown parameters can be determined. A description of LUNAR, including a list of the models used for computing a standard solution (such as Ocean Tides, Solid Earth Tides, etc.) along with a list of all parameters which are determined including the biases to station positions, is given in our previous study (Singh et al., 2021). Any parameters which are additionally fixed or estimated (compared to the standard model of LUNAR) are mentioned in this paper.

2.1. LLR data

For this study, 28093 NPs over the time span April 1970 - April 2021 were used. The distribution of the NPs has a big impact on the determination of various parameters. Non-uniform data distribution is one of the reasons for correlations between solution parameters (Williams et al., 2009). From 2015, many NPs were measured using laser pulses of infra-red (IR) wavelength, due to which ranging near new and full Moon became possible (Chabé et al., 2020) for OCA and WLRS. This leads to a better coverage of the lunar orbit over the synodic month, i.e. the time span in which the Sun, the Earth, and the Moon return to a similar constellation again. With a better coverage of the lunar orbit, it is possible to perform a more uniform estimation of ERPs. Fig. 1 shows the temporal distribution of the

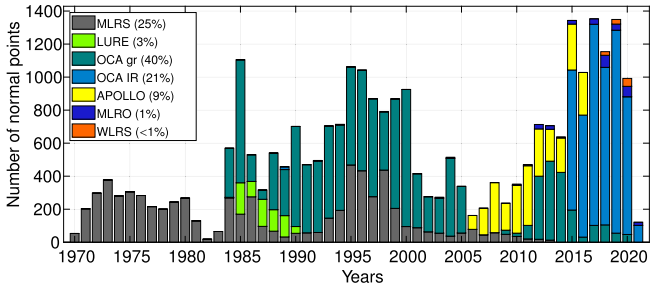

Fig. 1. Distribution of the 28,093 normal points over the time span April 1970 - April 2021. The percentages of the contribution of the respective observatories are given in the legend. The three observatories McDonald, MLRS1 and MLRS2 are linked in the analysis and listed here as 'MLRS'. OCA measurements with laser wavelength of $\lambda = 694.3$ nm and $\lambda = 532$ nm are listed as 'OCA gr'.

measured NPs since 1970. In the analysis, the three observatories McDonald, MLRS1, and MLRS2 are linked by local ties and analysed together, and are therefore listed in the figure as MLRS. OCA measurements with laser wavelength of $\lambda = 684.3$nm and $\lambda = 532$nm are listed in the figure as OCA green. As given in the legend of Fig. 1, more than 60% of the NPs were observed by OCA (40% with green and 21% with IR laser light). In the most recent years, only OCA and APOLLO provided regular NPs, and MLRO and WLRS only contributed a few NPs. For the year 2020, 84% of the NPs were measured by OCA in IR. Therefore, with this distribution of NPs, the overall analysis is dominated by the OCA NPs.

The measured NPs are used as observations in the analysis. They are treated as uncorrelated for the stochastic model of the least-squares adjustment and are weighted according to their measurement accuracies (provided by the observatories).

2.2. ERP a-priori data and estimation

In LUNAR, for a-priori EOP values, the KEOF COMB2019 series (Ratcliff & Gross, 2020) is used until 0h UTC 01.01.1983 and the IERS EOP 14 C04 series is used from 0h UTC 02.01.1983 onward. The differences between KEOF COMB2019 and IERS 14 C04 series are of a few μas for the PMC and a few μs for ΔUT1 after January 1, 2000. Before 2000, these differences are up to a few ms for ΔUT1 and a few mas for the PMC. Further details about the differences between IERS 14 C04 series and the COMB series can be found in (Ratcliff & Gross, 2020) and is briefly discussed in Section 2.3. This implementation of two different EOP time series within LUNAR is done as the COMB2019 series includes LLR data in its formation, and therefore fits our LLR analysis better (until end of 1982). After 01.01.1983, the differences we obtain in our LLR residuals between solutions using the two series (separately in two calculations) become small, and the differences in the estimated parameters between the two calculations were smaller than the uncertainty of the parameters, therefore we use the IERS 14 C04 to benefit from its shorter latency period. Using KEOF COMB2019 until end of 1982 and IERS 14 C04 series afterwards for LLR analysis is not uncommon, and was also applied by Pavlov et al. (2016) and Viswanathan et al., (2016).

As the rotation matrix between the Earth fixed International Terrestrial Reference System (ITRS) and the space fixed Geocentric Celestial Reference System (GCRS) includes the PMC and ΔUT1 in its calculation, these can be estimated from LLR analysis, as shown by Dickey et al., (1985); Müller (1991); Biskupek (2015). We refer the reader to Biskupek (2015) Eq. 5.43 - Eq. 5.53 for the equations of calculation of the partial derivatives of ERPs (used for the adjustment). The most recent results of ERP from LLR have been discussed by Biskupek (2015) and Hofmann et al. (2018). Biskupek (2015) discussed the results of the different possible methods to obtain ERP from LUNAR (selecting time spans or specific nights for which ERP are estimated) for 20047 NPs (1970–2013). The uncertainty of ΔUT1 achieved by Biskupek (2015) was a maximum of 0.14 ms (70 day period of estimation), and the uncertainty of the PMC was in the range of 30–90 mas (for different combinations of observatories from which the PMC were estimated). x_p and y_p were estimated separately by Biskupek (2015), due to their high correlations with each other. Hofmann et al. (2018) discussed the results of estimation of the ΔUT1 for 23261 NPs (1970–2016), achieving an uncertainty under 0.089 ms when estimating ΔUT1 from all observatories, and under 0.044 ms when estimating ΔUT1 from only OCA and APOLLO.

The ERP estimation from other techniques leads to better results than those from LLR, due to the availability of much more data and a better global coverage. The uncertainties achieved from different space geodetic techniques are given in Table 1, where it can be seen that the best results of the PMC are from GNSS, primarily due to dense network of its stations. The sensitivities of the space geodetic techniques are different for various EOPs, and not all techniques can determine all parameters.

Since 2015, IR NP measurements are available from OCA. These enable a better coverage of the lunar orbit and obtain more NPs per night, leading to a better and more stable estimation of ERPs from LLR, which achieves better uncertainty (i.e. lower value) compared to previous results. For ERPs determination from the LLR analysis,

Table 1
Uncertainties of the ERPs obtained from different space geodetic techniques (Sciarretta et al., 2010; Schuh and Behrend, 2012; Capitaine, 2017; Zajdel et al., 2020; Raut et al., 2022).

Technique	Parameters	
	PMC	ΔUT1
VLBI	50–80 μas	3–5 μs (24h), 15–20 μs (intensive)
SLR	10–30 μas	–
GNSS	5–20 μas	–

the whole dataset of NPs is pre-analysed. Here, different configurations can be taken into account (such as selecting NPs from different stations, different time spans, etc.), thereby making it possible to vary the minimum number of NPs per night and to estimate ERPs from the data of all observatories or only for a single observatory. Table 2 gives details of the subsets which were created for this study (based on different configurations), and the abbreviations we use to refer to these subsets.

As shown in Fig. 1, the number of NPs has significantly risen over the past few years, implying that more NPs were recorded per night, and that they were recorded for more nights. Despite having more NPs per night over the past years, it is currently still difficult to estimate PMC and ΔUT1 together due to their high correlation with each other. Therefore, in the current study, either PMC (x_p and y_p, separately and simultaneously) or ΔUT1 were determined, where the other values were fixed to the a-priori ERP series. It is also difficult to determine ERPs with the coordinates and velocities of the observatories together for one night (due to their correlations), therefore, the velocities of the observatories were fixed to the ITRF2014 solution values (https://itrf.ign.fr/en/solutions/itrf2014). As APOLLO observatory is not included in the ITRF2014 solution, we used the velocity for White Sands GNSS observatory (DOMES number: 49884S001) as the replacement.

The selection of nights was based on the observatory/observatories where the NPs were measured from (only from APOLLO, only from OCA, or from all observatories). We considered three sub-samples: with the minimum number of NPs per night as 5, 10, and 15 NPs (see Table 2). As the time span of only one of the subsets starts before 01.01.1983 (cut-off of using COMB2019 series in LUNAR), the a-priori ERP data used for all other subsets in this study is from the IERS 14 C04 series.

Preliminary studies showed that the uncertainties of the estimated parameters determined in our LLR adjustment were too small. Hofmann et al. (2018) described that despite a sophisticated analysis model, some small random and systematic effects still remained in the residuals of the solution from LUNAR. Random errors occur due to the overall measurement accuracy of LLR. Such errors differ for different nights, and also depend on the observatory the NPs are recorded from. They can amount to 1–2 cm in the LLR residuals. Systematic errors occur due to the imperfect realisation of the reference system from LLR, the constellation of observing a LLR NP (i.e. one observatory tracks one reflector at one instant), unmodelled effects (such as the effect of geocenter motion on LLR residuals, inclusion of asteroids in ephemeris calculation), inaccuracy of atmospheric delay models for observations at low elevation, etc. These effects also differ for each observation (for example, because LLR observations are performed at different and mostly high elevations) and can amount to about 1–2 cm in the LLR residuals. Additionally, the ERP values are fixed to those from the a-priori ERP series for all nights when sufficient LLR NPs are not available, which may lead to an underestimation of the error. To account for these unmodelled effects and further model deficiencies, the results are given with an estimated realistic error. It is computed as three times the formal error obtained from the adjustment procedure (standard deviation) which is equally used for all estimated parameters. This factor of three was obtained by performing multiple calculations (not a part of this study) by keeping various sets of parameters fixed and comparing the adjusted parameters from different calculations. Here, we also considered the uncertainties of these parameters reported by other LLR analysis groups. A smaller (i.e. better) uncertainty was obtained when more parameters were adjusted (compared to when fewer were adjusted). A list of all non-ERP parameters (other than station velocities) which were adjusted in this study are mentioned in Appendix A of Singh et al. (2021). Based on these investigations, we came to the conclusion that using three times the formal error provides a more realistic error estimate. Therefore, all uncertainties for ERPs are given as 3σ values in the following sections.

2.3. Differences between ERP time series from different sources

As different ERP time series have different combination strategies, use different software packages, and have differ-

Table 2
Details of the data subsets which were created for this study along with their time spans and abbreviations used for them.

Obs.*	NPs per night	No. of nights	Abbreviation used	Time span
APOLLO	5	261	Apollo05	04.06.2006–26.10.2016
	10	63	Apollo10	29.03.2008–24.10.2016
OCA	5	1320	OCA05	07.04.1984–30.03.2021
	10	714	OCA10	08.04.1984–24.03.2021
	15	355	OCA15	12.04.1984–26.12.2020
All	5	1975	All05	15.05.1971–30.03.2021
	10	914	All10	29.09.1983–24.03.2021
	15	450	All15	08.04.1984–19.01.2021

* Observatory/Observatories

ent sub-network of the ITRF2014, they show differences to each other. As mentioned above, the ERP between KEOF COMB2019 and IERS 14 C04 series are also slightly different. Fig. 2 and Fig. 3 show the differences between the ERP values of the two time series after 2000 and the uncertainties (i.e. standard errors) of the ERP values reported by each series.

From Fig. 2 and Fig. 3 it can be seen that the uncertainties of the ΔUT1 values reported by both series are smaller than the differences between them. Additionally, Bizouard et al. (2018) stated that the uncertainties reported by ERP time series from different space geodetic techniques are smaller than the differences between them, and discussed it as an indication of underestimated errors. Similarly large differences and small uncertainties were also reported by Fey et al., 2015; Hellmers et al., (2019); Schartner et al., (2022) etc. The differences between ERP time series from various sources can be attributed to several factors, such as different analysis strategies, differences in the realisation of the Terrestrial Reference System (TRS) and Celestial Reference System (CRS), different combination strategies of data from multiple sources, etc. The differences in the ERP values obtained from LLR and that of the a-priori series used are discussed in more detail in Section 3 and Section 4.

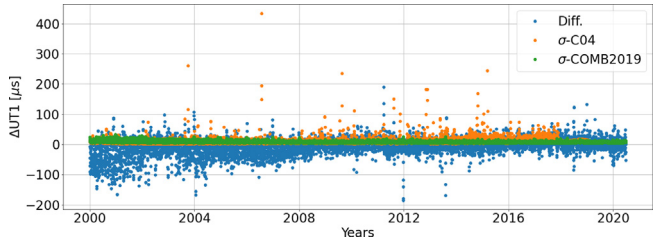

Fig. 2. Differences between ΔUT1 values of KEOF COMB2019 and IERS 14 C04 series and the uncertainties reported by them, after 2000.

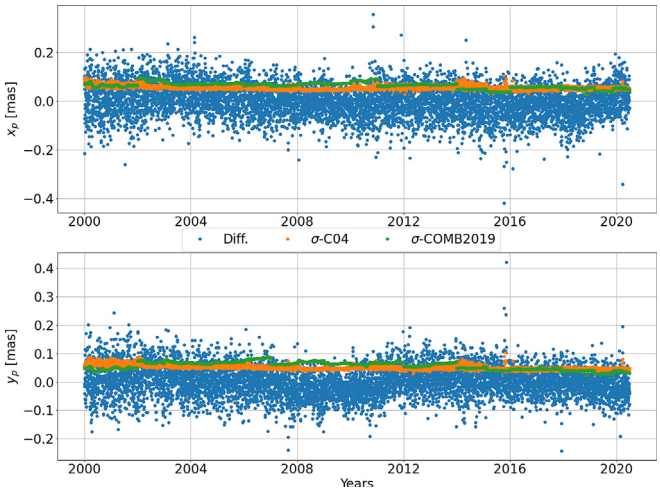

Fig. 3. Differences between x_p and y_p values of KEOF COMB2019 and IERS 14 C04 series and the uncertainties reported by them, after 2000.

2.4. Non-tidal loading data

The IERS 2010 conventions (Petit and Luzum, 2010) do not recommend the addition of NTL deformations in the calculation of the displacement of a reference point, as their modelling accuracy is low and their impact on the geodetic parameters compared to other deformations is small. However, their inclusion can be beneficial in geodetic analyses, as pointed out in recent studies (Glomsda et al., 2020; Singh et al., 2021).

In this study, we use the NTL provided by the International Mass Loading Service (IMLS; http://massloading.net/). It provides three non-tidal loadings (atmosphere: NTAL, ocean: NTOL, and hydrological: HYDL), which occur due to redistribution of masses in atmosphere, oceans, and land water. For further details we refer the reader to our previous study (Singh et al., 2021), where we discussed the effect of NTL as observation level corrections in LUNAR, and gave the details of the differences of the NTL data from different data centres, described the different components of the NTLs, including discussions on specifics such as resolution, numerical weather models used for each loading, etc. Overall, from that study, we concluded that the addition of NTL in LUNAR, primarily from the IMLS, leads to small benefits in reduction of the WRMS of LLR residuals, reduced the annual signal visible in the LLR residuals, and improved the estimation of station coordinates.

The loading deformation can be defined in a centre of figure (CF) frame (realised from the positions of geodetic stations on the solid Earth) or centre of mass (CM) frame (centre of orbiting satellites). This is controlled by the choice of degree-one load Love numbers, which enter the Green's function summation (Petrov and Boy, 2004; Dill and Dobslaw, 2013; Petrov, 2015) to calculate the effect of NTL. For further details on the differences between CM and CF, we refer to Sun (2017). In our LLR analysis, the a-priori station positions are aligned to the CM frame and therefore the loadings used in this study were chosen in the CM frame.

3. Estimation of ΔUT1

As mentioned in 2.2, the nights for which the ERP are estimated are categorised into different subsets. The ΔUT1 values were estimated for the nights of these subsets, using a-priori values from the combination of KEOF COMB2019 and IERS 14 C04 series, as described above. In the subsections that follow, we discuss the results of the estimated values of ΔUT1 and their uncertainty, their correlations with various parameters, and the effect of NTL on ΔUT1. Additionally, the results are published as Singh and Biskupek (2022).

For the estimation of ΔUT1, the velocities of the LLR observatories are fixed to ITRF2014 solution values, and the values of the PMC (x_p and y_p) are fixed to their a-priori values.

3.1. Estimated values

For the estimation of ΔUT1, the uncertainty of the estimated values becomes better (i.e. smaller standard deviations) over the years. This is due to the improved accuracy of the NPs measured over the years, primarily due to the improved accuracy of the OCA green laser data, the highly accurate IR NP data (starting 2015), and the highly accurate APOLLO data (starting 2006). The differences of the estimated values from LUNAR to the values of the a-priori ERP time series also become smaller over the time span, indicating the close agreement of the ΔUT1 values from the different space geodetic techniques (VLBI and LLR) with highly accurate data, thereby also verifying each other.

Fig. 4 shows the uncertainty of the ΔUT1 values for the subsets All05, All10, and All15, and Fig. 5 shows the uncertainty of the ΔUT1 values for the subsets OCA05, OCA10, and OCA15. As the uncertainty of the ΔUT1 values show a significant improvement (i.e. smaller values) in the recent years, we split the figure of each subset into two time spans, setting a break at 0h UTC 01.01.2000 (henceforth, '2000.0'). Fig. 6 shows the differences of the ΔUT1 values of LLR and the a-priori ERP time series (after 2000.0) for the subsets All05, All10, and All15. Additionally, Table 3 shows the WRMS values of all subsets considered in this study and the WRMS of the differences of the estimated values to the values of the a-priori ERP time series, where the weights correspond to the number of NPs which contributed to the ΔUT1 calculation per night. The values given in Table 3 are also split into two time spans, to show the differences in the estimation from the overall time span to the new data and to stress upon the best possible quality of the estimation from LLR.

It can be seen from Table 3 that the uncertainty of the estimated ΔUT1 values are smaller than the differences to the a-priori ERP time series. This is not uncommon, as mentioned in Section 2.3. The differences (estimated ΔUT1 values from LLR to the a-priori ERP time series, see Fig. 6) are due to multiple reasons. A part of these differences may occur because of the different realisations of the CRS from VLBI and LLR. Another part of these differences may be caused due to the difference in the network of the few LLR observatories compared to the large geodetic network used by the IERS C04 and the COMB2019 series for determining the ERPs. As also the coordinates of the LLR observatories are adjusted, the small LLR network may absorb certain errors which leads to deviations from the ITRF2014 solution and then also has an impact on the ΔUT1 determination. In the results shown, the

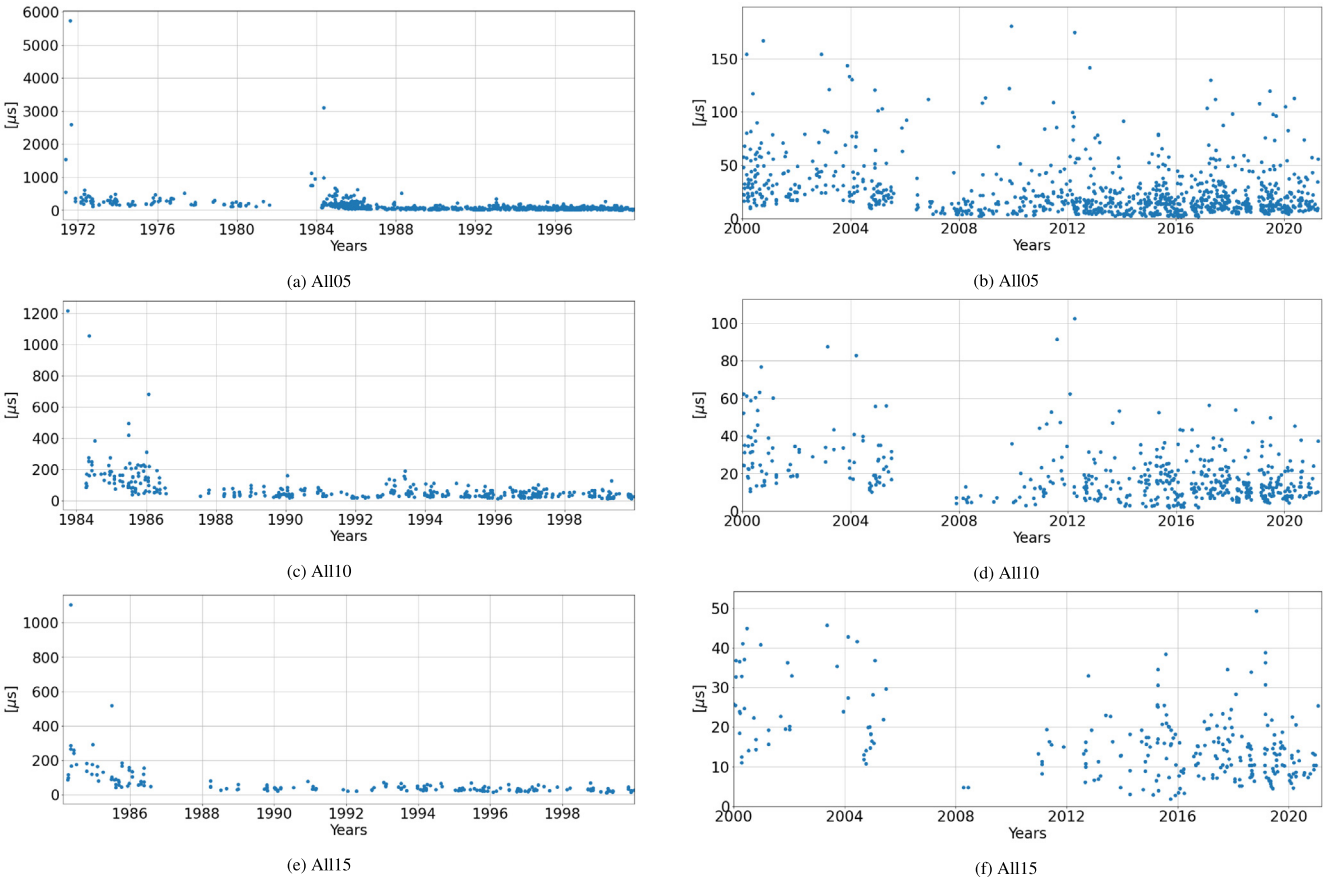

Fig. 4. Uncertainty of the estimated values of ΔUT1 for the subset All05, All10, and All15: in (a), (c), and (e) from the beginning of the dataset until 2000.0, and in (b), (d), and (f) from 2000.0 until the end of the dataset. Note the differences in the range of the axes for each sub-figure.

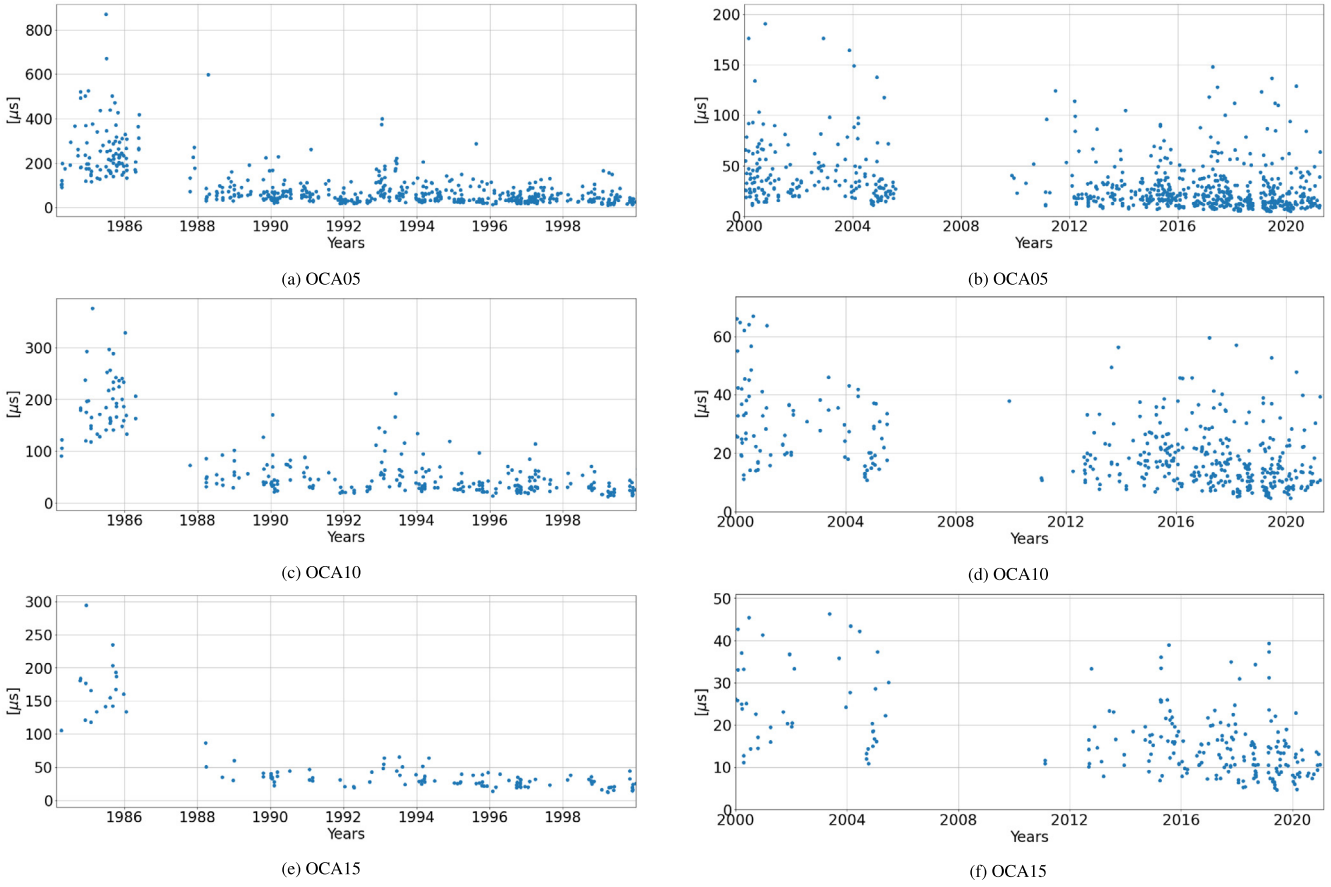

Fig. 5. Uncertainty of the estimated values of ΔUT1 for the subset OCA05, OCA10, and OCA15: in (a), (c), and (e) from the beginning of the dataset until 2000.0, and in (b), (d), and (f) from 2000.0 until the end of the dataset. Note the differences in the range of the axes for each sub-figure.

velocities of the LLR observatories were fixed to the ITRF2014 solution. Additionally, we also ran tests (results are not shown in this paper) where the velocities of the observatories were adjusted (thereby causing further deviation from the LLR network to the ITRF2014 solution, and aligning more to the LLR observations). There we noticed that the uncertainties of the estimated ΔUT1 values of all subsets were slightly smaller, but the correlations between the estimated ΔUT1 values and the positions of the LLR observatories were higher. Another part of the differences could arise as the ΔUT1 values from LLR are often averaged over a maximum time span of 12-hours (as LLR NPs can only be observed at night), while ΔUT1 values from VLBI are averaged over a 24-hours time span. Additionally, a part of the differences could be due to systematic errors in our calculation, such as unaccounted correlations between NPs as well as due to the specific network constellation of the stations and reflectors and the available time periods of LLR measurements. Moreover, as both the COMB2019 and the C04 series are individually a combined product of different space geodetic techniques, this combination also contributes to the improvement of all EOPs. As the results presented in this study are only from LLR analysis, a small part of the differences may occur due to the difference in obtaining the final ΔUT1 values. Generally, the differences of the estimated ΔUT1 values from LLR to the a-priori ERP time series become smaller with a stricter selection criteria (see Fig. 6), which also leads to a more stable and better solution. None of the subsets for which the ΔUT1 values were estimated showed an offset in the differences to the a-priori values (see Fig. 6, differences stay close to and around zero) indicating that there is no systematic deviation from the a-priori time series.

From Fig. 4, Fig. 5, and Table 3, it can be seen that the stricter the selection criteria (i.e. only those nights selected for ERP estimation with a higher number of minimum NPs per night), the better the results. However, it must also be noted that the improvement in the results with the strict selection criteria is more stark in the results until 2000.0, and leads to less improvement in the results after 2000.0, indicating that the very strict selection criteria is needed for data with low accuracy and that with the improvement of the accuracy of the NPs, a less strict selection criteria of the nights can be chosen. Additionally, it can be seen from Table 3 that the solution from the subsets of nights chosen from all observatories performs worse than the solution from the subsets of nights chosen from OCA only for the results before 2000.0. This is due to the reason that the accuracy of the NPs involved in the respective time spans of the subsets is significantly better from OCA compared

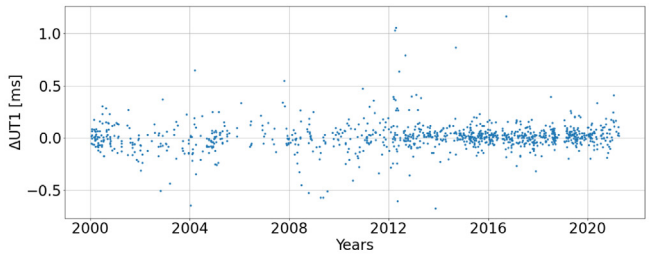

(a) All05

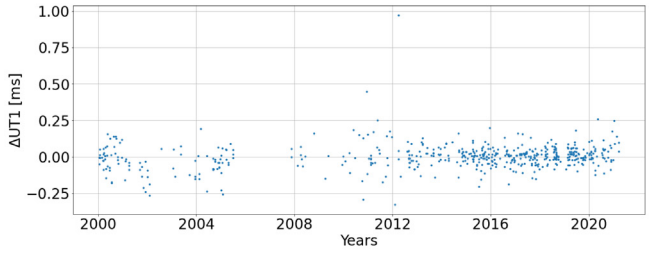

(b) All10

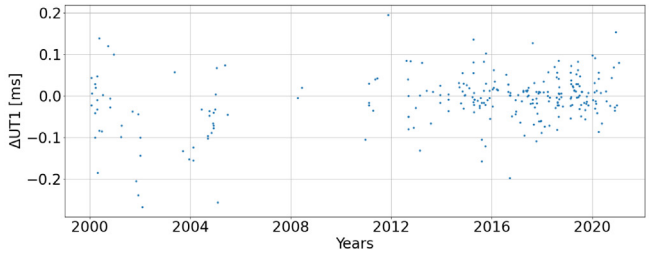

(c) All15

Fig. 6. Differences of the estimated LLR ΔUT1 values of the subsets All05, All10, and All15 (after 2000.0) to the ΔUT1 values of the a-priori ERP series.

Table 3
WRMS values of the uncertainty of ΔUT1 values obtained from different subsets ('3σ' in table), and the WRMS of the changes to ΔUT1 values (i.e. differences of estimated values to the values from the a-priori ERP time series ('Diff.' in table)) for the results from the beginning of any dataset until 2000.0 and the results after 2000.0.

	Before 2000.0 [μs]		After 2000.0 [μs]	
Subset	3σ	Diff.	3σ	Diff.
Apollo05	–	–	24.49	206.78
Apollo10	–	–	24.13	162.98
OCA05	118.54	277.33	31.49	85.81
OCA10	89.64	214.18	21.38	64.88
OCA15	72.15	181.27	17.53	54.16
All05	217.14	388.09	28.08	115.35
All10	114.66	257.41	20.95	80.78
All15	104.13	223.63	17.03	59.38

to when NPs from all observatories are chosen. However, when considering the results of all solutions after 2000.0, the results from the solutions of the 'All' subsets perform better than those from the solutions of the 'OCA' subsets, as the accuracy of the NPs (in this time span) from all observatories is comparable and the solutions of 'All' subsets benefit from having more data and having a global coverage of the NPs involved and including the very good APOLLO data.

Using the radius of Earth (at the equator) as 6378 km, 10 μs corresponds to 4.6 mm on the Earth's surface, implying that the best possible (and current) uncertainty of estimation of ΔUT1 (subset All15, after 2000.0) from LLR corresponds to 7.8 mm spatial resolution on Earth's surface. Compared to the best possible spatial resolution on Earth surface obtained from VLBI of 1.5 mm - 2.5 mm, LLR still lags behind VLBI, however the addition of more data from a different space geodetic technique could be beneficial for some applications. Additionally, the results from LLR can be used to verify the results from VLBI.

3.2. Correlations

The correlations of different parameters which are estimated in LUNAR with the ERP of the different estimated nights (henceforth, only 'correlations', in this section) were briefly discussed by Biskupek (2015). In this study, as mentioned before, the velocities of the LLR observatories were kept fixed to the ITRF2014 solution values.

One of the benefits of estimating the ERPs from only one observatory (compared to estimating from all observatories) is that it leads to a reduction in the correlations estimated within LUNAR, as also visible by Table 4, where we show the value of the maximum correlation of ΔUT1 for any night with any non-ERP parameter, obtained from each subset.

Overall, most parameters show no or very low correlation with the ΔUT1 values of any night. For the subsets from all observatories, the highest correlation, from all three subsets, of 80%, 70%, and 30% is with the y-coordinate of WLRS. The parameters, from all three 'All' subsets, which show more than a 30% correlation with the ΔUT1 values of any night are: the coordinates and/or biases of APOLLO, MLRS, LURE, OCA, and WLRS. Additionally, the x-coordinate of the L1 reflector shows a 30% correlation only for the subset All05. For the subsets from OCA, the parameters (from all three OCA subsets) which show more than a 20% correlation with the ΔUT1 values of any night are only the coordinates and biases of OCA. For the subsets from APOLLO, the parameters (from both APOLLO subsets) which show more than a 30% correlation with the ΔUT1 values of any night are the coordinates and biases of APOLLO. Additionally, for

Table 4
The maximum correlation of ΔUT1 of any night with any non-ERP estimated parameter, obtained from each subset.

Subset name prefix	Subset name suffix		
	05	10	15
Apollo	50%	30%	–
OCA	40%	20%	20%
All	80%	70%	30%

the subset Apollo05, the x-coordinate of OCA and the x-coordinate of the L1 reflector shows a 30% correlation.

Overall, the correlation between ΔUT1 values and the positions of LLR observatories is as expected. Additionally, the correlations with parameters such as the coordinates of lunar reflector disappear (or become smaller, and therefore irrelevant) when implementing the stricter selection criteria (10 or 15 NPs per night).

3.3. Effect of NTL on ΔUT1

As there are correlations between the station coordinates and ΔUT1, and as the addition of NTL lead to small benefits in our previous study, we decided to test the effect of including NTL in the ERP determination from LUNAR. Here, we added NTL only from IMLS, as it performed the best in LLR analysis (Singh et al., 2021). We represent the combination of its three components (NTAL, NTOL, and HYDL) as NTSL. The effect of NTL, as expected, is of similar - small - magnitude on the estimated ΔUT1 values from all subsets for which the calculations were performed. In Fig. 7, we show the effect when adding NTSL to the standard solution for the estimation of ΔUT1 from the subset All15. Additionally, in Table 5, we show the WRMS values of the uncertainty obtained for the estimation of ΔUT1 from the subsets OCA10, OCA15, All10, and All15 for the standard solution and the IMLS NTSL solution. The NTSL solution improves the uncertainty by 0.9% for both the 'All' subsets, and by 0.2% and 0.4% for the OCA10 and OCA15 subsets respectively.

As the effect of adding NTSL is similar for the whole time span (see Fig. 7), its effect on the results of the estimation of ΔUT1 does not change significantly when considering the entire time span of any subset, or only the time span which includes NPs with higher accuracy. Additionally, the inclusion of NTSL does not change the correlations, compared to the standard solution, at all. In Fig. 8, we show a comparison of the effect of NTSL on ΔUT1 values (absolute values) with the uncertainties of the estimation of ΔUT1 values for the results after 2000.0 (for the subset All15), as the uncertainties in this time span are significantly better than before 2000.0. For the subset All15, shown in Fig. 8, the WRMS of the effect of NTSL is 11.54 μs, and the WRMS of the uncertainty of ΔUT1 is

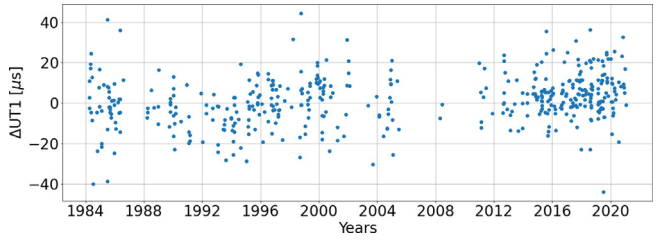

Fig. 7. Difference of the ΔUT1 values from the NTSL solution (NTSL from IMLS) to the ΔUT1 values from the standard solution for the subset All15 (i.e. ΔUT1 NTSL - ΔUT1 Standard).

Table 5
WRMS values of the uncertainty of ΔUT1 for the standard and the IMLS NTSL solution for the subsets OCA10, OCA15, All10, and All15.

Subset	Std [μs]	NTSL [μs]
OCA10	57.63	57.51
OCA15	43.63	43.47
All10	75.62	74.93
All15	67.25	66.63

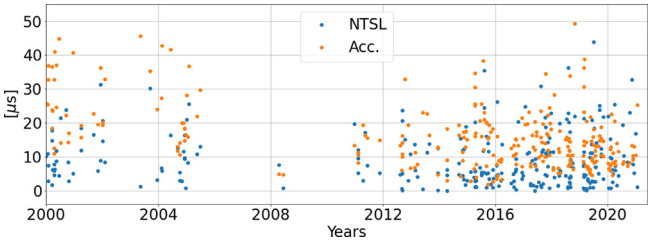

Fig. 8. Absolute values of the effect when adding of NTSL on ΔUT1 values (in blue) and the uncertainties of the estimated ΔUT1 values (in orange) for the subset All15, after 2000.0.

17.03 μs (see Table 3). Even though its effect is not significantly larger than uncertainties obtained of ΔUT1 values, we assess that there is a small improvement in the overall uncertainty of the estimated ΔUT1 values when including the NTSL (see Table 5). The improvement of the results due to the addition of IMLS NTSL is in sync with the findings from our previous study (Singh et al., 2021).

4. Estimation of terrestrial pole offsets

The PMC were estimated (for the nights of all subsets, Table 2), using a-priori values from the combination of KEOF COMB2019 and IERS 14 C04 series, as described above. In the subsections that follow, we discuss the results of the estimated values of x_p and y_p and their uncertainties, their correlations with each other and with other parameters, and the effect of NTL on them. Additionally, the results are published as Singh and Biskupek (2022).

For the estimation of x_p and y_p, the velocities of the LLR observatories were fixed to the ITRF2014 solution values, as it was also done for ΔUT1 estimation (see Section 3), and the values of ΔUT1 were fixed to their a-priori values.

4.1. Estimated values

The estimation of x_p and y_p (following the least-squares adjustment) gives the possibility of estimating x_p and y_p separately (i.e. only x_p or only y_p), or simultaneously (i.e. both x_p and y_p). In the previous results of x_p and y_p estimation from LUNAR (Biskupek, 2015), the estimation was done separately, as the correlation between the x_p and y_p values (of the same night) is high, and the estimated values were deemed to be more realistic when the adjustment was performed separately. With the expansion of the LLR

dataset over the past years (providing a longer time series), more NPs recorded per night, and improved coverage of the lunar orbit mainly because of the benefits of using IR laser pulses from OCA, the estimation of x_p and y_p simultaneously has benefited. In this study, we estimate the PMC simultaneously and separately, for all subsets mentioned in Table 2, and compare the results. In Table 6, we give the WRMS values of the uncertainty of x_p and y_p achieved, and the WRMS values of the differences of the estimated values to the a-priori ERP time series, where the weights correspond to the number of NPs which contributed to the calculation of the PMC per night. Additionally, as we did for ΔUT1 values, we split the results of PMC into two time spans, setting a break at 2000.0, for each subset, due to the stark improvement in the involved NPs and the results obtained over the LLR time span.

Fig. 9 shows the uncertainty of the PMC values (estimated simultaneously) for the subsets All05, All10, and All15, also split into two time spans, with a break at 2000.0. Fig. 10 and Fig. 11 show the differences of the estimated values of the PMC to the a-priori ERP time series after 2000.0. The mentioned figures and Table 6, give manifold results, discussed below.

As the x-axis for the polar motion is defined by the Greenwich meridian, and the y-axis is defined by the line joining the 90° meridian (see Fig. 2 of Combrinck (2009)), OCA is (and other European observatories would be) more sensitive to the estimation of x_p compared to y_p, whereas APOLLO is (and other American observatories would be) more sensitive to the estimation of y_p compared to x_p. This can also be seen by Table 6, where the WRMS values of the uncertainty of the estimated x_p values is better than the WRMS of the estimated y_p values, for the results after 2000.0 (for the 'OCA' and 'All' subsets). This is, however, not visible for the results before 2000.0, because of the combination of the worse accuracy of the NPs involved along with the high sensitivity of OCA to the x-axis. The results of x_p show a higher improvement between the split subsets (before and after 2000.0), compared to y_p (for example, WRMS values of x_p improves by 86.54% from 14.79 mas to 1.99 mas for the subset OCA10, whereas the WRMS value of y_p improves by 76.95% from 11.41 mas to 2.63 mas, for simultaneous calculation). As described in Section 2.1, the LLR data is not evenly distributed with OCA contributing to over 60% of the NPs, leading to better estimation of x_p from the subsets which consider NPs from all observatories as well, as most nights in the three subsets from all observatories are from OCA.

As it was also the case for ΔUT1 values, the differences to the a-priori ERP time series arise due to many different aspects. A part of these differences are due to the special properties of the different space geodetic techniques used to obtain the PMC values. The PMC values from LLR are often averaged over a maximum time span of 12-hours compared to an average over 24-hours time span from other techniques, contributing to another part of the

Table 6
WRMS values of the uncertainties of the x_p and y_p values obtained from different subsets ('3σ' in table), and the WRMS values of the changes to x_p and y_p values (i.e. differences of estimated values to the values from the a-priori ERP time series ('Diff.' in table)) for the results from the beginning of the dataset until 2000.0 in (a) and from 2000.0 until the end of the dataset in (b). The APOLLO subsets are not mentioned in (a) as both these subsets start after 2000.0.

Subset	x_p and y_p [mas]				Only x_p [mas]		Only y_p [mas]	
	3σ		Diff.		3σ	Diff.	3σ	Diff.
	x_p	y_p	x_p	y_p	x_p	x_p	y_p	y_p
(a) Before 2000.0								
OCA05	20.28	16.60	6.34	6.24	15.81	5.65	11.96	4.74
OCA10	14.79	11.41	4.43	3.56	12.76	4.54	9.30	3.56
OCA15	11.90	8.11	4.53	3.23	11.06	4.35	7.24	3.18
All05	37.98	28.31	38.01	24.42	20.13	16.96	17.71	13.33
All10	19.41	15.88	5.56	6.95	15.05	6.58	10.46	4.39
All15	18.23	17.40	5.60	7.75	13.55	3.68	10.15	3.35
(b) After 2000.0								
Apollo05	9.96	10.67	18.39	9.70	3.46	4.48	2.08	2.72
Apollo10	7.68	7.64	6.40	4.91	3.20	3.83	2.49	2.29
OCA05	3.71	5.23	1.98	2.42	2.18	1.28	3.05	1.38
OCA10	1.99	2.63	1.02	0.86	1.55	1.07	2.07	1.02
OCA15	1.54	1.94	0.94	0.71	1.34	0.98	1.70	0.95
All05	5.43	8.17	8.49	6.25	2.60	2.18	4.21	1.76
All10	2.91	3.08	2.26	1.36	1.67	1.60	1.94	1.16
All15	1.55	1.90	1.09	0.79	1.30	1.18	1.63	1.01

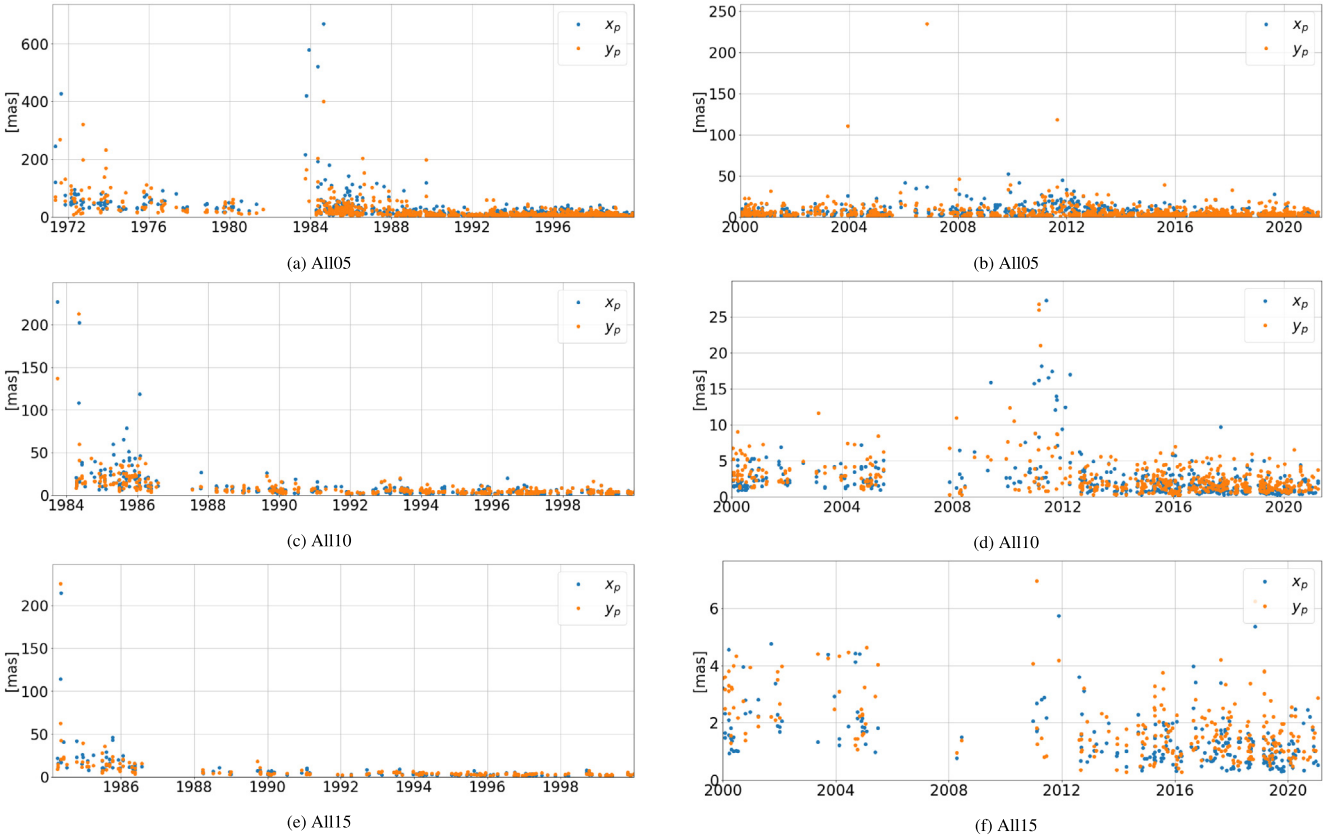

Fig. 9. Uncertainty of the estimated values of PMC (estimated simultaneously) for the subset All05, All10, and All15: in (a), (c), and (e) from the beginning of the dataset until 2000.0, and in (b), (d), and (f) from 2000.0 until the end of the dataset. Note the differences in the range of the axes for each sub-figure.

differences. As the PMC from the other space geodetic techniques (GNSS, VLBI, etc.) have lower uncertainties than those obtained from LLR, and additionally due to the combination of the time series of different space geodetic techniques, the results of PMC from LLR and those of the a-priori ERP time series differ from each other. From Table 6 it can be seen that the differences to the a-priori ERP time series are smaller than the uncertainties of the estimated PMC values. Some differences might be caused by the difference in the networks and by systematic errors in our calculation, as addressed above. Generally, similar to ΔUT1 estimation, the differences of the estimated PMC values from LLR to the a-priori ERP time series become smaller with a stricter selection criteria. None of the subsets for which the PMC values were estimated showed an offset in the differences to the a-priori values (see Fig. 10 and Fig. 11, differences stay close to and around zero) indicating that there is no systematic deviation from the a-priori time series.

Other than to avoid high correlation between the estimated PMC of the same night, the individual estimation of x_p and y_p also helps see whether the estimation of both x_p and y_p is stable or not. As seen in Table 6, the WRMS values of the uncertainties of x_p and y_p change the most for the subsets made from selection of 5 NPs per night, and change the least for selection of 15 NPs per night, indicating that the calculations with selection of only 5 NPs per night are not as stable as those with a higher number of NPs selected per night. Additionally, it can be seen that the results for the subsets from APOLLO change drastically when estimating x_p and y_p separately, compared to their estimation simultaneously, even though the NPs from APOLLO are the most accurate, amongst all NPs. This indicates that the estimation of the PMC is more stable when the number of nights for which the estimation is performed is higher.

For PMC, 1 mas corresponds to 3 cm spatial resolution on Earth surface, implying that the current and best possible spatial resolution of the PMC from LLR (subset All15, after 2000.0, PMC calculated separately) is at 3.9 cm for x_p and at 4.89 cm for y_p on Earth's surface. Compared to the spatial resolution obtained from other space geodetic techniques, such as GNSS, the results of PMC estimation from LLR lag far behind.

4.2. Correlations

As mentioned before, when estimating the PMC simultaneously, the values of x_p and y_p in the same night are correlated to each other. These correlations can be as high as

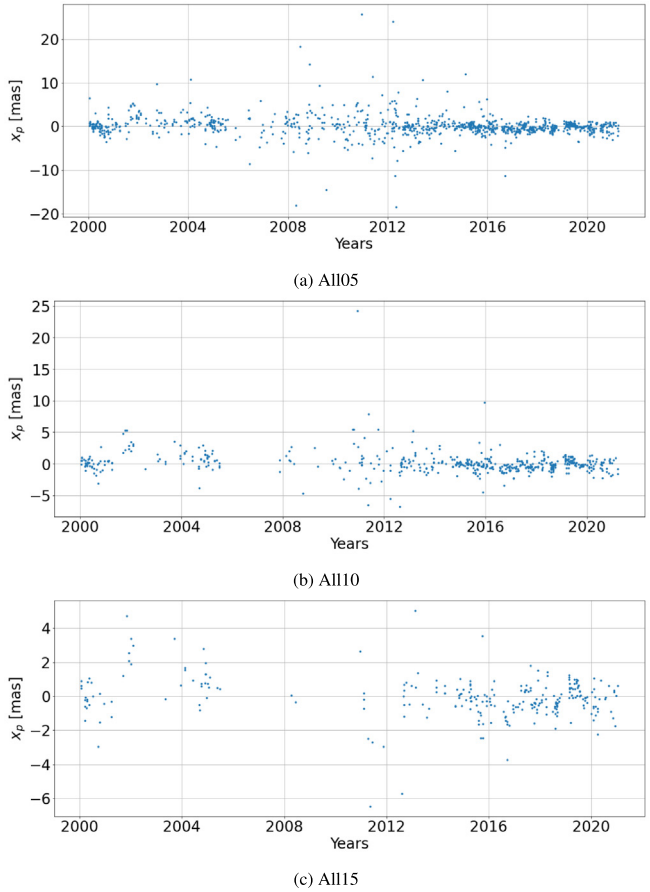

Fig. 10. Differences of the estimated LLR x_p values of the subsets All05, All10, and All15 (after 2000.0) to the x_p values of the a-priori ERP series (estimation of only x_p).

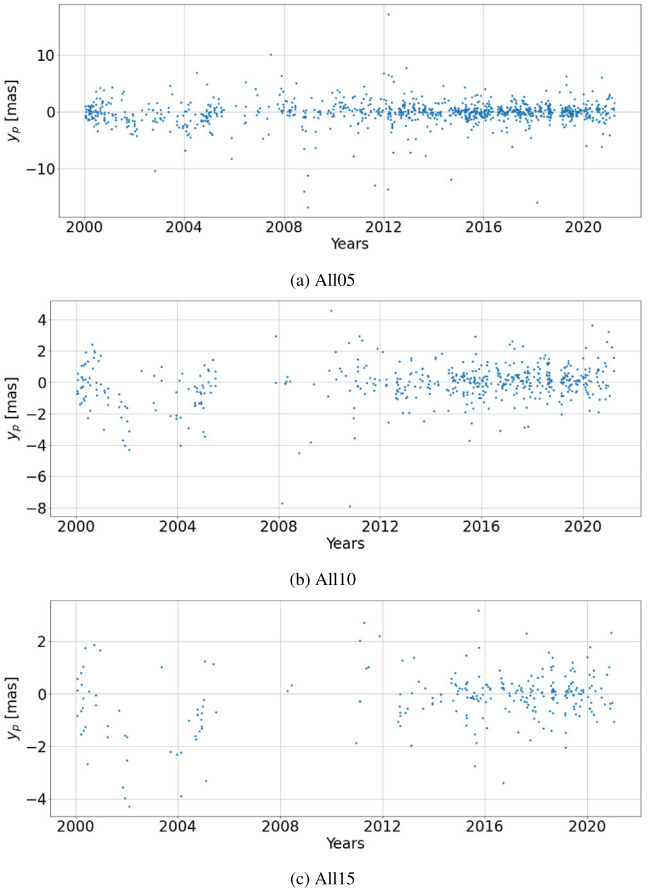

Fig. 11. Differences of the estimated LLR y_p values of the subsets All05, All10, and All15 (after 2000.0) to the y_p values of the a-priori ERP series (estimation of only y_p).

100% for the subsets with 5 and 10 NPs per night, indicating that the estimation of the PMC simultaneously in these cases leads to unstable results. The trend followed by all subsets is the same, i.e., the correlations of the subsets chosen with 5 NPs per night are the highest, where the PMC of many nights show a 100% correlation with each other. With the selection of 15 NPs per night, none of the nights (for OCA15, shown in Fig. 12) show a correlation of 100% with each other, proving the benefit of the strict selection criteria of subsets for ERP estimation from LLR. However, even with 15 NPs per night, the correlations of the x_p and y_p estimated in the same night with each other are very high.

For the correlation of the estimated x_p and y_p with the non-ERP parameters of LUNAR, the trend followed is the same as that for the estimation of ΔUT1 values, i.e., the correlation of the estimation from 'All' subsets is higher than the correlation of the estimation of ERP from nights selected from any one observatory. In Table 7, we show the value of the maximum correlations of x_p and y_p of any night with any non-ERP parameter for each subset.

As it was the case with correlations of ΔUT1 with non-ERP parameters, most parameters show either no or very low correlation with the estimated x_p and y_p. The parameters

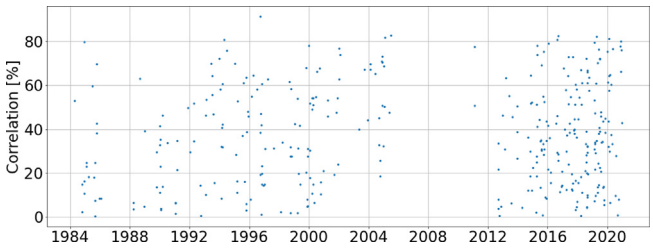

Fig. 12. Correlation of x_p and y_p estimated in the same night with each other, from the subset OCA15.

which show the maximum correlations, whether the PMC are estimated simultaneously or separately, stay the same. The highest correlations from the subset All05 and All10 are with the position of MAUI and MLRS. For the subset All15, the highest correlations are with the position of WLRS. Overall, the parameters which show a 40% correlation or more with either x_p and y_p are the station coordinates and/or biases of the LLR observatories. For OCA05 and OCA10 subsets, the highest correlation reach up to 50%, where, 30% or higher correlation is achieved only by the coordinates and/or biases of OCA. For Apollo05, the maximum correlations reach up to 60%, where the parameters

Table 7
The maximum correlations of x_p and y_p of any night with any non-ERP estimated parameter, obtained from each subset.

Subset name prefix	Subset name suffix		
	05	10	15
(a) x_p, estimation of PMC simultaneously			
Apollo	60%	40%	–
OCA	50%	30%	30%
All	100%	100%	40%
(b) y_p, estimation of PMC simultaneously			
Apollo	60%	30%	–
OCA	30%	20%	10%
All	90%	90%	30%
(c) x_p, estimation of only x_p			
Apollo	50%	30%	–
OCA	50%	30%	30%
All	80%	80%	40%
(d) y_p, estimation of only y_p			
Apollo	60%	30%	–
OCA	40%	20%	10%
All	70%	60%	40%

which show a 30% or higher correlation are only the coordinates and/or biases of APOLLO. For Apollo10, only the coordinates and/or biases of APOLLO show a 20% or more correlation, reaching a maximum of 40%.

The parameters which show a correlation with the PMC are the same, whether the estimation is done separately or simultaneously. The percentage by which they are correlated also stays very similar, as can also be seen in Table 7 (specially for the subsets with the strict selection criteria of 15 NPs per night). The difference in correlations between these two cases is that more nights show a correlation with those parameters when the estimation of PMC is done separately. Some effect is also absorbed by the correlation between the x_p and the y_p of the same night.

4.3. PMC signal analysis

The polar motion has three major components: Chandler wobble, annual oscillation, and a drift along the 80° West meridian. When applying a Fourier transformation of the PMC from the IERS 14 C04 series (not shown), signals with an annual period and a Chandler period are visible. As the LLR NPs are temporally unevenly distributed, a Fourier transformation of the estimated PMC values is not possible. To perform a spectral analysis of a non-uniformly distributed data, we used the Lomb-Scargle (LS) periodogram. However, to obtain a very clear distribution, a high sampling rate and uniformity of data samples is beneficial (VanderPlas, 2017), which is not given in LLR dataset. Due to these reasons, the LS power (not shown) at the annual and Chandler frequency component did not show similar high peaks as the Fourier transformation of the PMC from the IERS 14 C04 series for all subsets. In the difference of the powers obtained from the LS periodograms of the a-priori PMC values and the estimated PMC values from LUNAR, no change of the signals was visible when estimating PMC (whether simultaneously or separately).

4.4. Effect of NTL on estimated values

As the station coordinates and PMC are also correlated, we checked the effect when adding NTL for the estimation of PMC from LUNAR, as we did for ΔUT1 estimation. Here, the effect of addition of NTL is only shown for the case where x_p and y_p were estimated separately. The NTL was added only from IMLS, as a combination of its three individual loading components: NTAL, NTOL, and HYDL. The combination of the three loadings is referred to as 'NTSL'. The effect of NTSL, as expected, is of similar - small - magnitude on the estimated PMC values from all subsets. In Fig. 13, we show the effect when adding NTSL to the standard solution for the estimation of PMC (separately) from the subset All15 (PMC estimated separately). Additionally, in Table 8, we show the WRMS values of the uncertainty obtained for the estimation of PMC from the subsets OCA10, OC15, All10, and All15 for the standard solution and the IMLS NTSL solution.

When adding the NTSL, there was no change observed in the correlations of the PMC with the non-ERP parameters of LUNAR. In our previous study (Singh et al., 2021), we discussed the benefit of reduction of the annual signal in LLR residuals when adding NTSL. However, as the data from the subsets is temporally extremely unevenly dis-

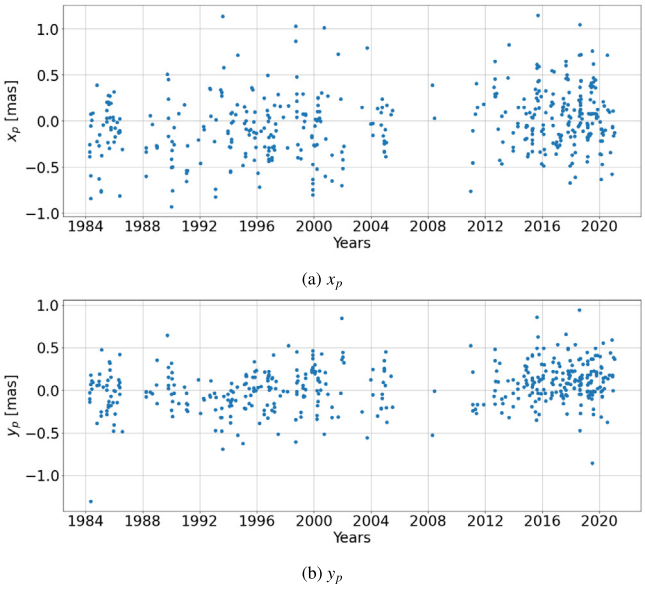

Fig. 13. Difference of the x_p and y_p values from the NTSL solution (NTSL from IMLS) to the x_p and y_p values from the standard solution for the subset All15 (i.e. x_p and y_p NTSL - x_p and y_p Standard). (x_p and y_p estimated in separate calculations).

Table 8
WRMS values of uncertainty of the PMC values for the standard and the IMLS NTSL solution for the subsets OCA10, OCA15, All10, and All15 (x_p and y_p estimated in separate calculations).

Subset	x_p [mas]		y_p [mas]	
	Std	NTSL	Std	NTSL
OCA10	7.92	7.88	5.95	5.90
OCA15	6.39	6.35	4.37	4.33
All10	9.77	9.68	6.90	6.83
All15	8.61	8.53	6.55	6.48

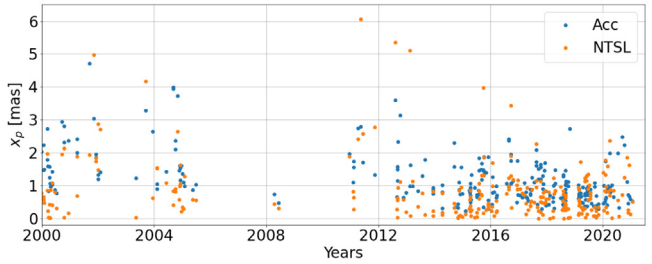

(a) x_p

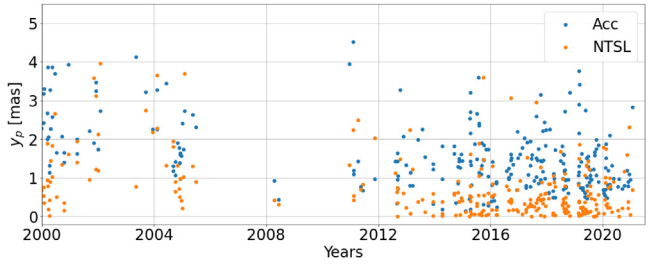

(b) y_p

Fig. 14. Absolute values of the effect of addition of NTSL on x_p and y_p and the values of uncertainties for the estimated x_p and y_p for the subset All15, after 2000.0 (x_p and y_p estimated in separate calculations).

tributed, any effect the addition of NTSL might have at the annual signal is masked by noise.

In Fig. 14, we show a comparison of the effect of NTSL on the PMC (absolute values) with the uncertainties of the estimation of x_p and y_p values for the results after 2000.0 for the subset All15, as the best uncertainties are obtained in this time span. It can be seen that the absolute effect of NTSL is significantly smaller than the uncertainties of the x_p and y_p values. In spite of the effect being smaller, there is a small improvement in the overall uncertainty of the estimated values when including the NTSL, see Table 8. Overall, the uncertainty of the PMC improves for the IMLS NTSL solutions (between 0.5% and 1.1% for all components). As mentioned previously, these changes are in sync with the findings from our previous study (Singh et al., 2021).

5. Conclusions and outlook

In this study, we estimated the Earth rotation parameters (Earth rotation phase, ΔUT1, and the terrestrial pole offsets, x_p and y_p), from LLR analysis for eight different subsets of nights in the LLR time span. We estimated the ERPs by performing a least-squares adjustment. For the analysis, we kept the velocities of the LLR observatories fixed to the ITRF2014 solution values, and estimated ΔUT1 and the PMC separately, to avoid high correlations between them. For the estimation of PMC, we estimated x_p and y_p simultaneously and separately. We discussed the differences of the estimated ERP results to the a-priori ERP time series, for the different subsets, analysed the uncertainty of their estimation, and additionally discussed the effect of addition of NTL on the ERP estimation.

Generally, the estimation of ERP shows a significant improvement over the time span of the subsets considered in this study, with the WRMS values of the uncertainty of the estimated values reducing to (almost) a third of its value when comparing the results before and after 0h UTC 01.01.2000. The best possible result of estimated ERP (on Earth's surface) is 7.8 mm (i.e. 17.03 μs) for ΔUT1 estimation, and about 4.4 cm for PMC (i.e. 1.30 mas for x_p and 1.63 mas for y_p). Compared to other space geodetic techniques, the results from LLR still lag behind, however are still important, as LLR is the only technique other than VLBI which can provide ΔUT1 values with some good accuracy to verify the VLBI results, especially if the LLR accuracy can further be improved in the future. From Table 3 and Table 6 it can be seen that the stricter selection criterion of a minimum of 15 NPs per night (compared to a minimum of 5 NPs per night) leads to smaller differences between results obtained from LLR and from the a-priori ERP time series. If more LLR NPs per nights can be obtained in the future, the agreement between the results of LLR and from other space geodetic techniques will further improve.

LLR is more sensitive to the estimation of ΔUT1 values than PMC values. This is due to low number of NPs per night used within the estimation, combined with the fact that changes per night are larger for ΔUT1 than for the PMC. Furthermore, due to the distribution of the LLR data (most NPs are measured from OCA), the estimation of PMC from LLR is more sensitive to x-direction than to y-direction. The values of the WRMS values of the uncertainty obtained from different subsets, shown in Table 6, where the values of x_p are smaller than y_p, and the improvement in the values of x_p is more significant than in y_p, when comparing the results from the old NPs (before 2000.0) to the results from the new NPs (after 2000.0).

For the estimation of PMC, with the estimation of x_p and y_p simultaneously and separately, we were able to assess the stability of the calculation. With the subsets which were selected with a strict selection criteria of either 10 or 15 NPs per night, and when the number of nights for which ERP were estimated was not too few (such as for the subset Apollo10, 63 nights) the results of the estimated x_p and y_p values were not too different from each other when estimated separately or simultaneously.

The estimated ERP are primarily correlated to the positions of the observatory the nights were selected from. With a more strict selection criteria (15 NPs per night

instead of 5 NPs per night), the correlations reduce significantly, however, this comes at the cost of having fewer nights at which the ERP can be estimated. The estimated PMC (when estimated simultaneously) are highly correlated to each other (x_p and the y_p values of the same night), with correlations going as high as 100%. These correlations come down to a highest of 80% with the strict selection criteria of 15 NPs per night from one observatory, however are still too high. With the less strict selection criteria of 5 NPs per night, the ERP show correlations up to 20% and 30% with some parameters such as reflectors, the rotational time lags of the Earth (diurnal and semi-diurnal, due to the tidal effect of the Moon), etc., which disappear (or become smaller, and therefore irrelevant) when implementing the stricter selection criteria.

The NTL was applied as observation level corrections in our LLR analysis and added as the combination of its three different loading constituents for mass redistribution in atmosphere, oceans, and land water from the IMLS dataset. The impact when adding the NTL on ERP estimation is smaller in magnitude than the uncertainties of the ERP values, for both ΔUT1 and PMC. However, it leads to about 1% improvement in the uncertainties obtained, and is therefore recommended to be added for ERP estimation.

With the more accurate and more frequent LLR data in future, possibly with the measurements using Differential Lunar Laser Ranging (DLLR) (Dehant et al., 2017; Turyshev et al., 2017; Viswanathan et al., 2021; Zhang et al., 2022), better results for ERP can be expected from LLR. The results of ΔUT1 may become competitive to VLBI if the expected DLLR accuracy of 30 μm might be realised in future. Results of ERP estimation from LLR will also improve if more observatories on Earth can track the Moon, for example, if dedicated transponders will be placed on the Moon. However the latency of LLR NPs or DLLR observations are still expected to be in the range of 1–2 months (at least). By a joint analysis of VLBI and LLR data, better results of ΔUT1 estimation can potentially be achieved.

Declaration of Competing Interest

The authors declare that they have no known competing financial interests or personal relationships that could have appeared to influence the work reported in this paper.

Acknowledgements

Current LLR data are collected, archived, and distributed under the auspices of the International Laser Ranging Service (ILRS) (Pearlman et al., 2019). We acknowledge with thanks that the processed LLR data, since 1969, has been obtained under the efforts of the personnel at the Observatoire de la Côte d'Azur in France, the LURE Observatory in Maui, Hawaii, the McDonald Observatory in Texas, the Apache Point Observatory in New Mexico, the Matera Laser Ranging observatory in Italy, and the Wettzell Laser Ranging System in Germany. This research was funded by the Deutsche Forschungsgemeinschaft (DFG, German Research Foundation) under Germany's Excellence Strategy EXC 2123 QuantumFrontiers, Project-ID 390837967. We would additionally like to thank Franz Hofmann for his contributions to LUNAR.

References

Bauer, R., 1989. Bestimmung von Parametern des Erde-Mond-Systems - Ein Beitrag zur Modellerweiterung und Bewertung, Ergebnisse -. Ph.D. thesis Technische Universität München. Deutsche Geodätische Kommission bei der Bayerischen Akademie der Wissenschaften, Reihe C, Nr. 353.

Biskupek, L., 2015. Bestimmung der Erdorientierung mit Lunar Laser Ranging. Ph.D. thesis Leibniz University Hannover, Deutsche Geodätische Kommission bei der Bayerischen Akademie der Wissenschaften, Reihe C, Nr. 742. doi:10.15488/4721.

Biskupek, L., Müller, J., Torre, J.-M., 2021. Benefit of New High-Precision LLR Data for the Determination of Relativistic Parameters. Universe 7 (2). https://doi.org/10.3390/universe7020034.

Bizouard, C., Lambert, S., Gattano, C., Becker, O., Richard, J.-Y., 2018. The iers eop 14c04 solution for earth orientation parameters consistent with itrf 2014. J. Geodesy 93. https://doi.org/10.1007/s00190-018-1186-3.

Capitaine, N., 2017. The Determination of Earth Orientation by VLBI and GNSS: Principles and Results. In: Arias, E.F., Combrinck, L., Gabor, P., Hohenkerk, C., Seidelmann, P.K. (Eds.), The Science of Time 2016. Springer International Publishing, Cham, pp. 167–196.

Chabé, J., Courde, C., Torre, J.-M., Bouquillon, S., Bourgoin, A., Aimar, M., Albanèse, D., Chauvineau, B., Mariey, H., Martinot-Lagarde, G., Maurice, N., Phung, D.-H., Samain, E., Viot, H., 2020. Recent Progress in Lunar Laser Ranging at Grasse Laser Ranging Station. Earth and Space. Science 7. https://doi.org/10.1029/2019EA000785, e2019EA000785.

Combrinck, L., 2009. Products of Space Geodesy and Links to Earth Science and Astronomy. https://doi.org/10.3997/2214-4609-pdb.241.combrinck_wl_paper1.

Dehant, V., Park, R., Dirkx, D., Iess, L., Neumann, G., Turyshev, S., Van Hoolst, T., 2017. Survey of Capabilities and Applications of Accurate Clocks: Directions for Planetary Science. Space Sci. Rev. 212 (3–4), 1433–1451. https://doi.org/10.1007/s11214-017-0424-y.

Dickey, J.O., Newhall, X.X., Williams, J.G., 1985. Earth Orientation From Lunar Laser Ranging and an Error Analysis of Polar Motion Services. J. Geophys. Res. 90. https://doi.org/10.1029/JB090iB11p09353.

Dill, R., Dobslaw, H., 2013. Numerical simulations of global-scale high-resolution hydrological crustal deformations. J. Geophys. Res. Solid Earth 118 (9), 5008–5017. https://doi.org/10.1002/jgrb.50353.

Egger, D. (1985). Systemanalyse der Laserentfernungsmessung. Ph.D. thesis Technische Universität München. Deutsche Geodätische Kommission bei der Bayerischen Akademie der Wissenschaften, Reihe C, Nr. 311.

Fey, A., Gordon, D., Jacobs, C., Ma, C., Gaume, R., Arias, F., Bianco, G., Boboltz, D., Böckmann, S., Bolotin, S., Charlot, P., Collioud, A., Engelhardt, G., Gontier, A.-M., Heinkelmann, R., Kurdubov, S., Lambert, S., Malkin, Z., Macmillan, D., Titov, O., 2015. The second realization of the international celestial reference frame by very long baseline interferometry. Astron. J.

Folkner, W., Williams, J., Boggs, D., Park, R., Kuchynka, P., 2014. The Planetary and Lunar Ephemerides DE430 and DE431. Interplanet. Netw. Prog. Rep, 196.

Gambis, D., Salstein, D., Lambert, S., 2011. Use of atmospheric angular momentum forecasts for ut1 predictions: Analyses over cont08. J. Geodesy 85, 435–441. https://doi.org/10.1007/s00190-011-0479-6.

Gleixner, H., 1986. Ein Beitrag zur Ephemeridenrechnung und Parameterschätzung im Erde-Mond-System. Ph.D. thesis Technische Univer-

sität München. Deutsche Geodätische Kommission bei der Bayerischen Akademie der Wissenschaften, Reihe C, Nr. 319.
Glomsda, M., Bloßfeld, M., Seitz, M., Seitz, F., 2020. Benefits of non-tidal loading applied at distinct levels in VLBI analysis. J. Geodesy 94 (90), 1–19. https://doi.org/10.1007/s00190-020-01418-z.
Hellmers, H., Thaller, D., Bloßfeld, M., Kehm, A., Girdiuk, A., 2019. Combination of vlbi intensive sessions with gnss for generating low latency earth rotation parameters. Adv. Geosci. 50, 49–56. https://doi.org/10.5194/adgeo-50-49-2019, URL: https://adgeo.copernicus.org/articles/50/49/2019/.
Hofmann, F., 2017. Lunar Laser Ranging – verbesserte Modellierung der Monddynamikund Schätzung relativistischer Parameter. Ph.D. thesis Leibniz University Hannover. Deutsche Geodätische Kommission bei der Bayerischen Akademie der Wissenschaften, Reihe C, Nr. 797.
Hofmann, F., Biskupek, L., Müller, J., 2018. Contributions to reference systems from Lunar Laser Ranging using the IfE analysis model. J. Geodesy 92, 975–987. https://doi.org/10.1007/s00190-018-1109-3.
Hofmann, F., Müller, J., 2018. Relativistic Tests with Lunar Laser Ranging. Class. Quantum Gravity 35-035015 (3). https://doi.org/10.1088/1361-6382/aa8f7a.
Kopeikin, S., Pavlis, E., Pavlis, D., Brumberg, V., Escapa, A., Getino, J., Gusev, A., Müller, J., Ni, W.-T., Petrova, N., 2008. Prospects in the orbital and rotational dynamics of the Moon with the advent of sub-centimeter lunar laser ranging. Adv. Space Res. 42 (8), 1378–1390. https://doi.org/10.1016/j.asr.2008.02.014.
Müller, J., 1991. Analyse von Lasermessungen zum Mond im Rahmen einer post-Newton'schen Theorie. Ph.D. thesis Technische Universität München. Deutsche Geodätische Kommission bei der Bayerischen Akademie der Wissenschaften, Reihe C, Nr. 383.
Müller, J., Biskupek, L., Hofmann, F., Mai, E., 2014. Lunar laser ranging and relativity. In: Kopeikin, S.M. (Ed.), Frontiers in relativistic celestial Mechanics, Applications and Experiments, 2. Walter de Gruyter, Berlin, pp. 103–156.
Müller, J., Biskupek, L., Oberst, J., Schreiber, U., 2009. Contribution of Lunar Laser Ranging to Realise Geodetic Reference Systems. In: Geodetic Reference Frames. International Association of Geodesy Symposia. Springer, Berlin Heidelberg, Berlin, Heidelberg, pp. 55–59. doi:10.1007/978-3-642-00860-3-8.
Müller, J., Hofmann, F., Biskupek, L., 2012. Testing various facets of the equivalence principle using lunar laser ranging. Class. Quantum Gravity 29, 184006. https://doi.org/10.1088/0264-9381/29/18/184006.
Müller, J., Murphy, T.W., Schreiber, U., Shelus, P.J., Torre, J.M., Williams, J.G., Boggs, D.H., Bouquillon, S., Bourgoin, A., Hofmann, F., 2019. Lunar Laser Ranging: a tool for general relativity, lunar geophysics and Earth science. J. Geodesy 93, 2195–2210. https://doi.org/10.1007/s00190-019-01296-0.
Murphy, T.W., 2013. Lunar laser ranging: the millimeter challenge. Rep. Prog. Phys. 76, 076901. https://doi.org/10.1088/0034-4885/76/7/076901.
Pavlov, D.A., Williams, J.G., Suvorkin, V.V., 2016. Determining parameters of Moon's orbital and rotational motion from LLR observations using GRAIL and IERS-recommended models. Celestial Mech. Dyn. Astron. 126, 61–88. https://doi.org/10.1007/s10569-016-9712-1.
Petit, G., Luzum, B. (Eds.) (2010). IERS Conventions 2010. Number 36 in IERS Technical Note. Frankfurt am Main: Verlag des Bundesamtes für Kartographie und Geodäsie.
Petrov, L., 2015. The International Mass Loading Service. http://arxiv.org/abs/1503.00191.
Pearlman, M.R., Noll, C.E., Pavlis, E.C., Lemoin, F.G., Combrink, L., Degnan, J.J., Kirchner, G., Schreiber, U., 2019. The ILRS: approaching 20 years and planning for the future. Journal of Geodesy 93, 2161–2180. https://doi.org/10.1007/s00190-019-01241-1.
Petrov, L., Boy, J.-P., 2004. Study of the atmospheric pressure loading signal in very long baseline interferometry observations. J. Geophys. Res. Solid Earth 109 (B3). https://doi.org/10.1029/2003JB002500.
Ratcliff, J.T., Gross, R.S., 2020. Combinations of Earth OrientationMeasurements: SPACE2019, COMB2019, and POLE2019. Technical Report JPL Publication 20–3 Jet Propulsion Laboratory.
Raut, S., Heinkelmann, R., Modiri, S., Belda, S., Balidakis, K., Schuh, H., 2022. Inter-comparison of ut1-utc from 24-hour, intensives, and vgos sessions during cont17. Sensors 22, 2740. https://doi.org/10.3390/s22072740.
Schartner, M., Plötz, C., Soja, B., 2022. Improvements and comparison of vlbi int2 and int3 session performance. J. Geodesy 96. https://doi.org/10.1007/s00190-022-01621-0.
Schuh, H., Behrend, D., 2012. VLBI: A fascinating technique for geodesy and astrometry. J. Geodyn. 61, 68–80. https://doi.org/10.1016/j.jog.2012.07.007.
Sciarretta, C., Luceri, V., Pavlis, E., Bianco, G., 2010. The ILRS EOP time series. Artif. Satellites 45, 41–48. https://doi.org/10.2478/v10018-010-0004-9.
Singh, V.V., Biskupek, L., 2022. Dataset: Earth Rotation Parameters from LLR with NPs for timespan 1970–2021. Research data repository of the Leibniz University Hannover. https://doi.org/10.25835/3h1r07a7.
Singh, V.V., Biskupek, L., Müller, J., Zhang, M., 2021. Impact of non-tidal station loading in LLR. Adv. Space Res. 67 (12), 3925–3941. https://doi.org/10.1016/j.asr.2021.03.018.
Sun, Y., 2017. Estimating geocenter motion and changes in the Earth's dynamic oblateness from GRACE and geophysical models. Ph.D. thesis TU Delft Physical and Space Geodesy. doi:10.4233/uuid:7-fe64dde-7fb5-4392-8160-da6f7916dc6b.
Turyshev, S.G., Shao, M., Hanh, I., Peng, M., Williams, J.G., Trahan, R., 2017. Advanced Laser Ranging for high-precision navigation and science investigations in Fundamental Physics. Innside, Bremen, Germany: 656th WE-Heraeus Seminar (Fundamental Physics in Space).
VanderPlas, J.T., 2017. Understanding the Lomb-Scargle Periodogram. Astrophys. J. Suppl. Ser. 236 (1), 16. https://doi.org/10.3847/1538-4365/aab766.
Viswanathan, V., Fienga, A., Manche, H., Courde, C., Torre, J.-M., Exertier, P., Laskar, J., 2016. Updates from INPOP ephemerides: Data reduction model and parameter estimation using IR LLR data from OCA.
Viswanathan, V., Mazarico, E., Merkowitz, S., Williams, J., Turyshev, S., Currie, D., Ermakov, A., Rambaux, N., Fienga, A., Courde, C., Chabé, J., Torre, J.-M., Bourgoin, A., Schreiber, K., Eubanks, M., Wu, C., Dequal, D., Dell'Agnello, S., Biskupek, L., Müller, J., Kopeikin, S., 2021. Extending Science from Lunar Laser Ranging. Bull. Am. Astron. Soc. 53. https://doi.org/10.3847/25c2cfeb.3dc2e5e4.
Viswanathan, V., Rambaux, N., Fienga, A., Laskar, J., Gastineau, M., 2019. Observational Constraint on the Radius and Oblateness of the Lunar Core-Mantle Boundary. Geophys. Res. Lett. 46, 7295–7303. https://doi.org/10.1029/2019GL082677.
Williams, J.G., Boggs, D.H., Folkner, W.M., 2013. DE430 Lunar Orbit, Physical Librations, and Surface Coordinates. Technical Report Jet Propulsion Laboratory, California Institute of Technology, Pasadena, CA, USA. Interoffice memorandum, IOM 335-JW, DB, WF-20130722-016.
Williams, J.G., Turyshev, S.G., Boggs, D.H., 2009. Lunar Laser Ranging Tests of the Equivalence Principle with the Earth and Moon. Int. J. Modern Phys. D 18 (7), 1129–1175. https://doi.org/10.1142/S021827180901500X.
Williams, J.G., Turyshev, S.G., Boggs, D.H., Ratcliff, J.T., 2006. Lunar laser ranging science: Gravitational physics and lunar interior and geodesy. Adv. Space Res. 37, 67–71. https://doi.org/10.1016/j.asr.2005.05.013.
Zajdel, R., Sosnica, K., Bury, G., Dach, R., Prange, L., 2020. System-specific systematic errors in earth rotation parameters derived from gps, glonass, and galileo. GPS Solutions 24. https://doi.org/10.1007/s10291-020-00989-w.
Zhang, M., Müller, J., Biskupek, L., 2020. Test of the equivalence principle for galaxy's dark matter by lunar laser ranging. Celest. Mech. Dyn. Astron. 132 (4), 25. https://doi.org/10.1007/s10569-020-09964-6.
Zhang, M., Müller, J., Biskupek, L., Singh, V.V., 2022. Characteristics of differential lunar laser ranging. Astron. Astrophys. https://doi.org/10.1051/0004-6361/202142841.